# Supplementary Information

## Strong suppression of gene conversion with increasing DNA double-strand break load delimited by 53BP1 and RAD52

**Emil Mladenov, Christian Staudt, Aashish Soni, Tamara Murmann-Konda, Maria Siemann-Loekes and George Iliakis[1]**

# Supplementary Figure Legends

**Figure S1. (A)** DSB repair kinetics generated by pulsed-field gel electrophoresis (PFGE) in exponentially growing chicken DT40 cells exposed to 80 Gy. DT40 cells have 1000-fold increased gene targeting efficiency suggesting increased GC efficiency. Included, in addition to results of wt DT40 cells, are also results obtained with a conditional knockout mutant of RAD51 and knockout mutants of RAD51B, RAD52 and Rad54. For every DT40 clone, a dose response curve was generated and used to calculate the dose equivalent (Deq) values. Data shown here have been extracted from figures of an earlier publication (1) and are summarized in a new way to support the reasoning of the present work. **(B)** As in (A) for actively growing wt and RAD54 deficient MEFs exposed to 20 Gy. Results extracted from an earlier publication (2). **(C)** As in (A) for wt Chinese hamster V79 and their *XRCC2* and *XRCC3* deficient mutants exposed to 20 Gy and sorted in $G_2$-phase before analysis by PFGE. Results extracted from an earlier publication (3). **(D)** As in (A) for wild-type (wt), V79 cells exposed to increasing doses of IR in the range between 20 - 80 Gy. Results extracted from an earlier publication (4). **(E)** As in (D) for the KU80 deficient mutant of CHO cells, *Xrs6* (4).

**Figure S2. (A)** Representative MIP images of A549 cells, stained used specific antibodies against Cyclin B1 (CycB1) to identify cells in late S/$G_2$-phase of the cell cycle. Cells are also stained for RAD51. Cells negative for Cyclin B1 without RAD51 foci are considered as $G_1$-cells. Cells negative for Cyclin B1, but positive for RAD51 foci are considered as early- or mid-S-phase cells, while cells slightly positive for Cyclin B1 with RAD51 foci are considered as late-S-phase cells. Cells clearly positive for Cyclin B1 with RAD51 foci are considered as $G_2$-phase cells and are included in the analysis. **(B)** Representative flow cytometry histograms of exponentially growing, $G_1$, S and $G_2$-phase centrifugal elutriation-enriched A549 cells. **(C)** Representative flow cytometry

histograms utilized to define the gates for $G_1$-, S- and $G_2$-phase cells in order to quantitate IR-induced γ-H2AX signal generation in a cell cycle specific manner.

**Figure S3. (A-B)** MIP images of γ-H2AX foci at $t_{max}$ in HCT116-WT and HCT116-LIG4$^{-/-}$ cells. **(C-D)** MIP images of RAD51 foci at $t_{max}$ in HCT116-WT and HCT116-LIG4$^{-/-}$ cells. **(E-F)** Histogram and dot plots of data obtained by quantitative image-based cytometry analysis (QIBC) of HCT116-WT and HCT116-LIG4$^{-/-}$ cells. The gates used to score γ-H2AX foci in a cell cycle specific manner are also indicated. For the current analysis EdU$^-$, $G_2$-cells were selected. **(G-H)** Histogram and dot plots of data obtained by QIBC for scoring RAD51 foci in HCT116-WT and HCT116-LIG4$^{-/-}$ cells. Other details as in (E-F).

**Figure S4. (A)** Western blot analysis of LIG4 level in HCT116-WT and HCT116-*LIG4*$^{-/-}$ cells using two specific antibodies against LIG4 (Ab1-mouse monoclonal Ab (D-8), Ab2-rabbit polyclonal Ab (HPA001334)). GAPDH levels serve as loading control. **(B)** γ-H2AX foci at $t_{max}$ as a function of IR dose in HCT116-WT and HCT116-*LIG4*$^{-/-}$, EdU$^-$, $G_2$-cells. In these cells, saturation of γ-H2AX foci occurs above 4 Gy owing to the larger size of foci forming. Therefore, only the linear range is used to estimate the number of DSBs forming per Gy. The lines represents linear regressions through the indicated points. **(C)** RAD51 foci at $t_{max}$ as a function of IR dose for EdU$^-$, $G_2$-phase, HCT116-WT and HCT116-*LIG4*$^{-/-}$ cells.

Data points represent the mean and standard deviation from two independent experiments.

**Figure S5. (A)** Standard curve used to estimate the absolute RAD51 protein amount in cellular extracts. Known amounts of purified RAD51 protein in the range between 5 and 200 ng were loaded on a SDS-PAGE gel and detected by western blotting. The right panel shows signal intensity of the RAD51 bands as a function of RAD51 concentration. Each lane also contains as a loading control 100 ng of purified KU70. **(B)** As in (A) in the range between 50 and 1000 ng

RAD51 protein. **(C)** Representative flow cytometry histograms of exponentially growing Capan1 cells, as well as of $G_1$- and $G_2$-phase-enriched populations obtained by centrifugal elutriation. **(D)** Western blot analysis of RAD51 distribution between chromatin (Lamin A/C positive) and soluble ($\alpha$-Tubulin positive) fractions in elutriated, $G_2$-enriched, Capan1 cells.

**Figure S6. (A)** $\gamma$-H2AX foci formation in CycB1$^+$, HA-AsiSI-ER, U2OS cells after administration of 4-OHT for the indicated time periods. **(B)** RAD51 foci formation in CycB1$^+$, HA-AsiSI-ER, U2OS cells after administration of 4-OHT for the indicated time periods.

Data points represent the mean and standard deviation from two independent experiments.

**Figure S7. (A)** Schematic representation of the DR-GFP reporter, specifically designed to detect GC repair events, integrated into DR-GFP, U2OS cells. GFP positive cells are measured 24h after *I-Sce*I transfection in untreated cells, as well as in cells where RAD51, CtIP or RAD52 were knocked-down, or DNA-PKcs inhibited by using 10 μM NU7441. Results shown are normalized to those of untreated controls. Representative western blots showing the level of RAD51 and RAD52 knockdown. **(B)** As in (A) for the SA-GFP, U2OS cells reporting SSA repair events **(C)** As in (A) for EJ2-GFP, U2OS cells reporting alt-EJ repair events. **(D)** Effect of IR applied at the indicated times and doses on the reading of the EJ2-GFP reporter. **(E)** As in (A) for EJ5-GFP, U2OS cells reporting NHEJ repair events. **(F)** Effect of IR applied at the indicated times and doses on the reading of the EJ5-GFP reporter.

Data points represent mean and standard deviation from three independent experiments.

**Figure S8. (A)** Representative flow cytometry histograms of EdU$^-$, $G_2$-phase, A549 cells showing an increase in RPA70 accretion on chromatin, a measure for DNA end resection. Data are obtained 3h after exposure to the indicated IR doses. S-phase cells in the population were pulse-labelled with EdU just before IR exposure. The analysis utilizes three parametric flow cytometry. PI

staining is used for DNA content analysis and allows definition of the cell cycle phases. EdU signal identifies cells in S-phase at the time of irradiation, as well as cells that progressed from S- to $G_2$-phase in the post-irradiation incubation interval. RPA70 signal increase above unirradiated controls quantitates DNA end resection. The results shown are specifically from $EdU^-$, $G_2$-phase cells, determined by applying the gates defined in (B and C). The gates select for the cells irradiated in $G_2$-phase and remaining in $G_2$-phase at the time of analysis **(B)** Upper panel: Dot plots showing RPA70 *versus* PI signals for cells exposed to 0, 2, and 4 Gy. Middle panels: Dot plots showing EdU *versus* PI signals in the same cell populations. Shown in these panels are also the gates applied for quantitating resection at different times after IR in $EdU^-$, $G_2$-cells. **(C)** As in (B) for cells exposed to 8, 16, 24, 48, and 72 Gy.

**Figure S9. (A)** Western blot analysis of phosphorylated form of KAP1 at Serine 824 (pKAP1-S824) in HA-AsiSI-ER, U2OS cells, 1h after exposure to 2 Gy, or 4h after administration of 4-OHT. The phosphorylated form of KAP1 validates formation of DSBs by IR, or AsiSI after its translocation to the nucleus. GAPDH serve as loading control. **(B)** Dose response curves of γ-H2AX foci in HA-AsiSI-ER, U2OS cells exposed to the indicated IR doses and scored at $t_{max}$ (1h). **(C)** Dose response curve of IR induced RPA70 foci in HA-AsiSI-ER, U2OS cells. **(D)** Dose response curve of IR induced accretion of RPA70 to chromatin in HA-AsiSI-ER, U2OS cells, measured by bivariate flow cytometry. Other details as in Figure S8.

**Figure S10. (A)** Western blot analysis of 53BP1 protein in *53BP1*$^{+/+}$ and *53BP1*$^{-/-}$ MES cells. **(B)** Flow cytometry histograms showing the cell cycle distribution of actively proliferating *53BP1*$^{+/+}$ and *53BP1*$^{-/-}$ MES cells, as well as of the corresponding $G_2$-enriched populations generated by centrifugal elutriation. **(C)** MIP images of RAD51 foci (green) at $t_{max}$ in $G_2$-enriched *53BP1*$^{+/+}$ and *53BP1*$^{-/-}$ MES cells. **(D and E)** Kinetics of RAD51 foci formation and decay in $G_2$-enriched,

*53BP1*$^{+/+}$ and *53BP1*$^{-/-}$ MES cells generated by centrifugal elutriation. Other details as in Figure 2B. **(F)** Ratio between RAD51 and 53BP1 foci in CycB1$^{+}$, $G_2$-phase, A549 cells. **(G)** Ratio between 53BP1 and γ-H2AX foci in CycB1$^{+}$, $G_2$-phase, A549 cells. The dashed line traces the ratio of RAD51 to γ–H2AX as shown in Figure 2E.

Data points represent mean and standard deviation from three independent determinations.

**Figure S11. (A)** MIP images of RAD51 foci (red) in *53BP1*$^{+/+}$ and *53BP1*$^{-/-}$ U2OS cells, generated by using high-throughput imaging platform (Metasystems). Blue lines delineate the nuclear area as determined by DAPI staining. To select for analysis specifically $G_2$-phase cells, cultures were pulse-labelled with EdU to identify and exclude S-phase cells. Here, RAD51 foci are scored in EdU$^{-}$ cells with $G_2$-phase DNA content, determined by DAPI staining. **(B)** Repair kinetics of RAD51 foci in EdU$^{-}$, $G_2$-phase, *53BP1*$^{+/+}$ U2OS cells exposed to 2, 4, and 8 Gy. **(C)** As in (A) for *53BP1*$^{-/-}$ U2OS cells. **(D)** As in (B), for *53BP1*$^{-/-}$ U2OS cells. **(E)** RAD51 foci at $t_{max}$ as a function of IR dose in *53BP1*$^{-/-}$ and *53BP1*$^{+/+}$ U2OS cells. 100-200 EdU$^{-}$, $G_2$-cells were scored for each point. Data shown are from two independent experiments.

**Figure S12. (A)** MIP images of γ-H2AX foci formation in A549 cells treated or not with RAD52i. **(B)** MIP images of 53BP1 foci formation in A549 cells treated or not with RAD52i. **(C and D)** Repair kinetics of RAD51 foci in CycB1$^{+}$, A549 cells treated or not with RAD52i. Other details as in Figure 2B. **(E and F)** As in (C and D) for EdU$^{-}$, $G_2$-cells mock-transfected or transfected with siRNA specific for RAD52.

# Supplementary Table

**Table S1. (A)** Statistical analysis of data presented in Figure 4D and 4E. A student t-Test was used to determine the p-value. P-values below 0.05 are shown in green, while p-values above 0.05 are shown in red. P-values between 0.05 and 0.058 are shown in light green. **(B)** Statistical analysis of data presented in Figures 4F and 4G for the indicated irradiated pairs. **(C and D)** Statistical analysis of data presented in Figure 4F and 4G for the indicated pairs. Other details as in (A).

## Supplementary References


1. Wang, H., Zeng, Z.-C., Bui, T.-A., Sonoda, E., Takata, M., Takeda, S. and Iliakis, G. (2001) Efficient rejoining of radiation-induced DNA double-strand breaks in vertebrate cells deficient in genes of the RAD52 epistasis group. *Oncogene*, **20**, 2212-2224.

2. Wu, W., Wang, M., Wu, W., Singh, S.K., Mussfeldt, T. and Iliakis, G. (2008) Repair of radiation induced DNA double strand breaks by backup NHEJ is enhanced in G2. *DNA Repair*, **7**, 329-338.

3. Wu, W., Wang, M., Mussfeldt, T. and Iliakis, G. (2008) Enhanced Use of Backup Pathways of NHEJ in $G_2$ in Chinese Hamster Mutant Cells with Defects in the Classical Pathway of NHEJ. *Radiation Research*, **170**, 512-520.

4. Iliakis, G., Mehta, R. and Jackson, M. (1992) Level of DNA double-strand break rejoining in Chinese hamster xrs-5 cells is dose-dependent: Implications for the mechanism of radiosensitivity. *International Journal of Radiation Biology*, **61**, 315-321.

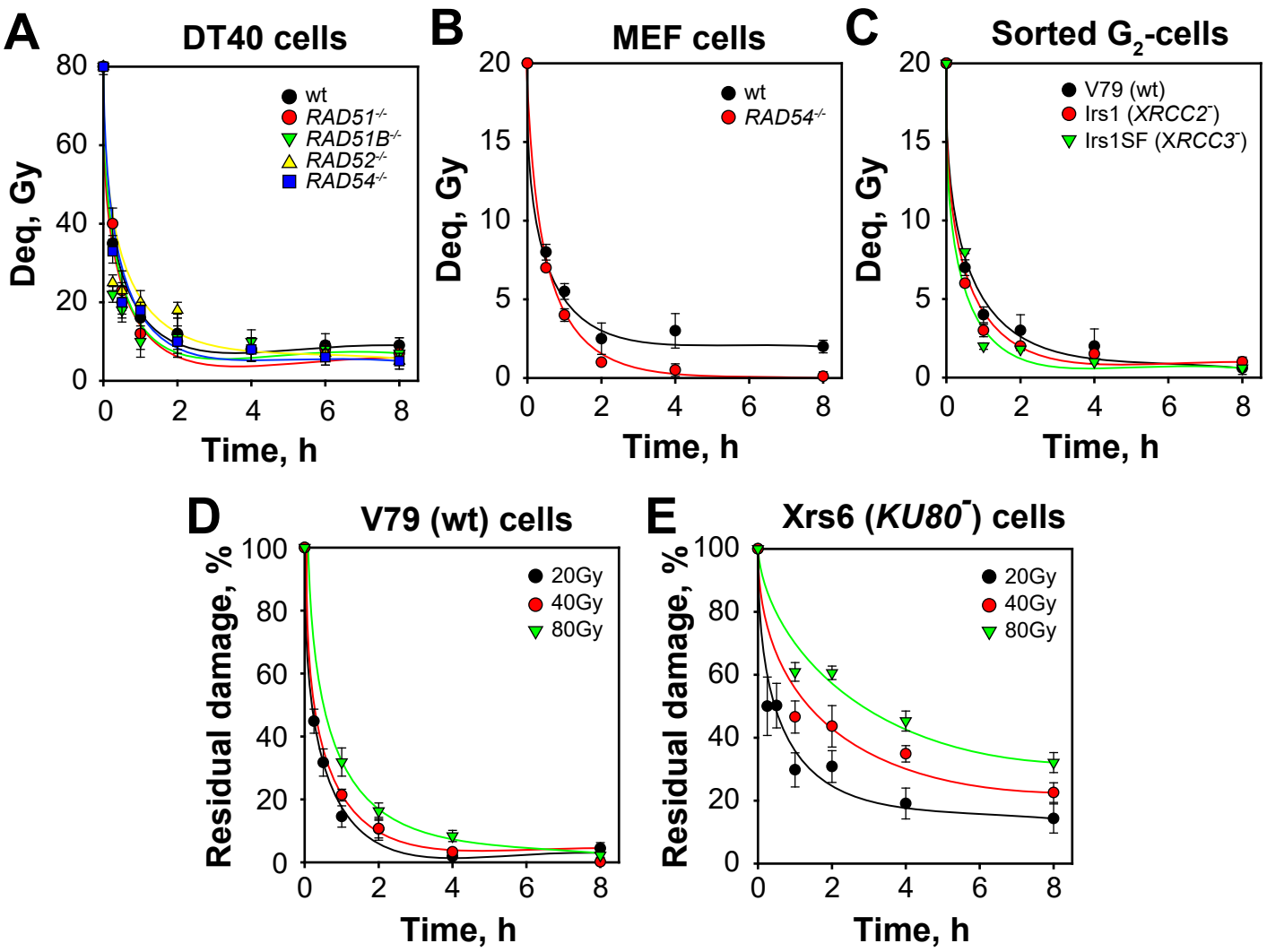


**Figure S1; Mladenov et al.**

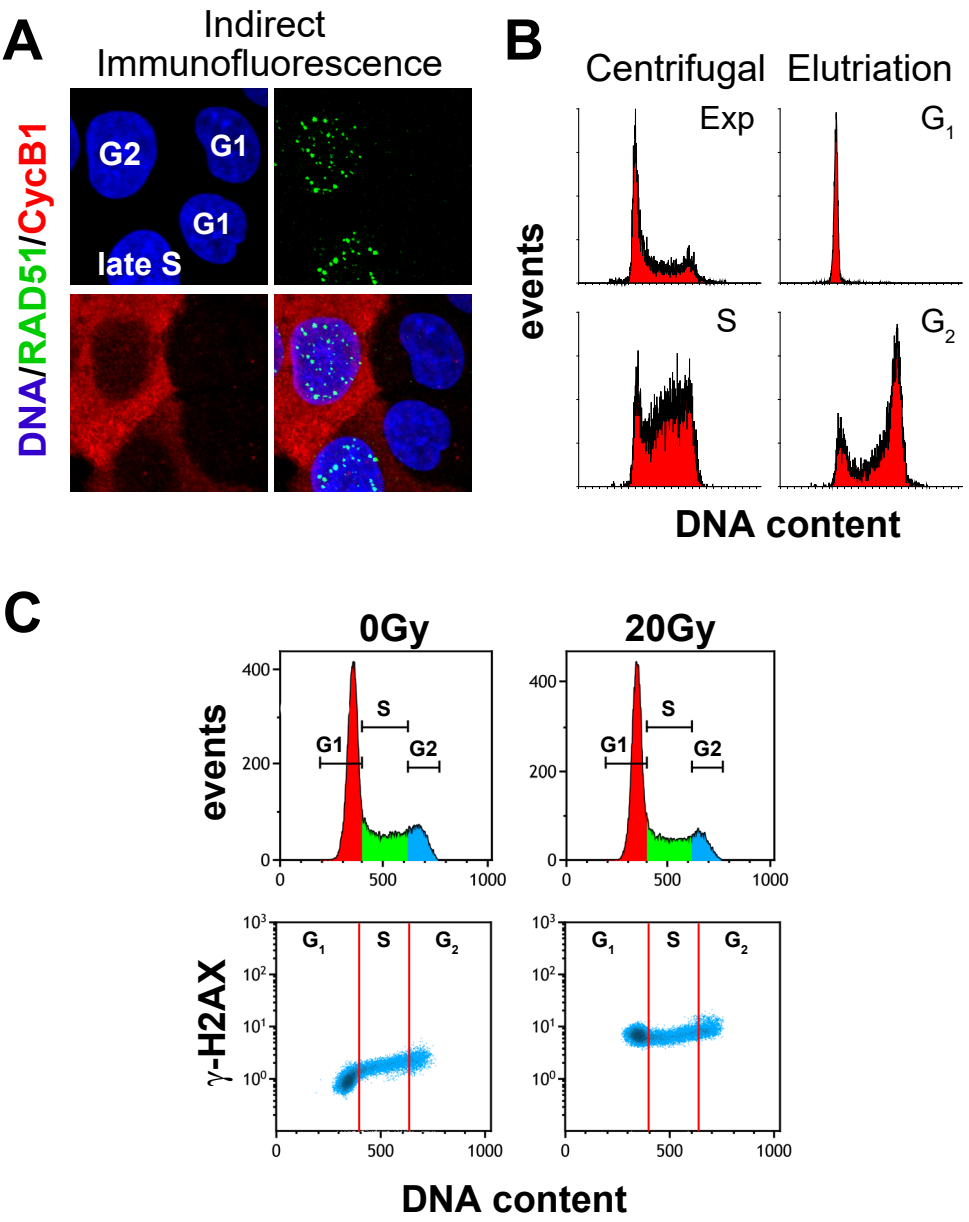


**Figure S2; Mladenov et al.**

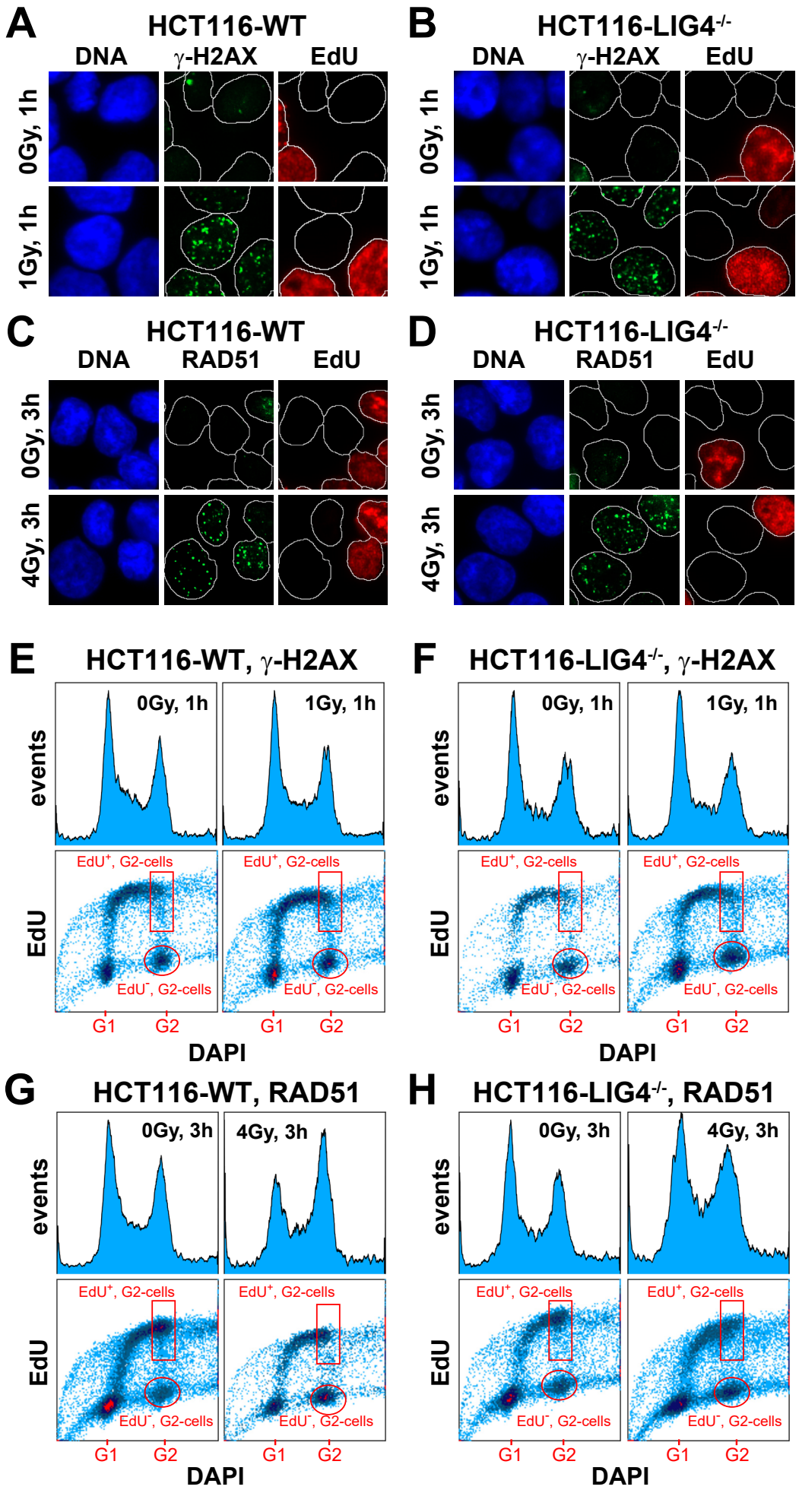


**Figure S3; Mladenov et al.**

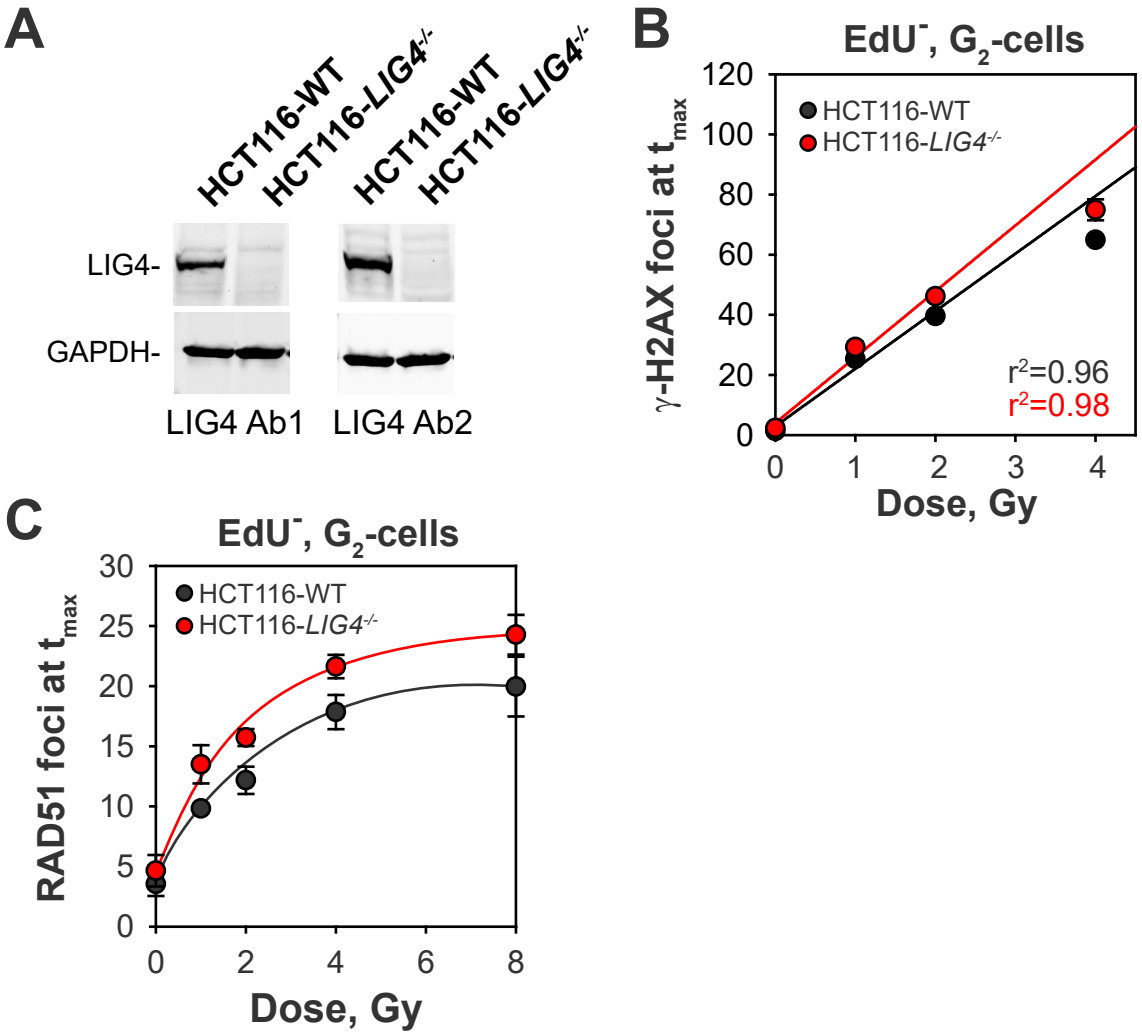


**Figure S4; Mladenov et al.**

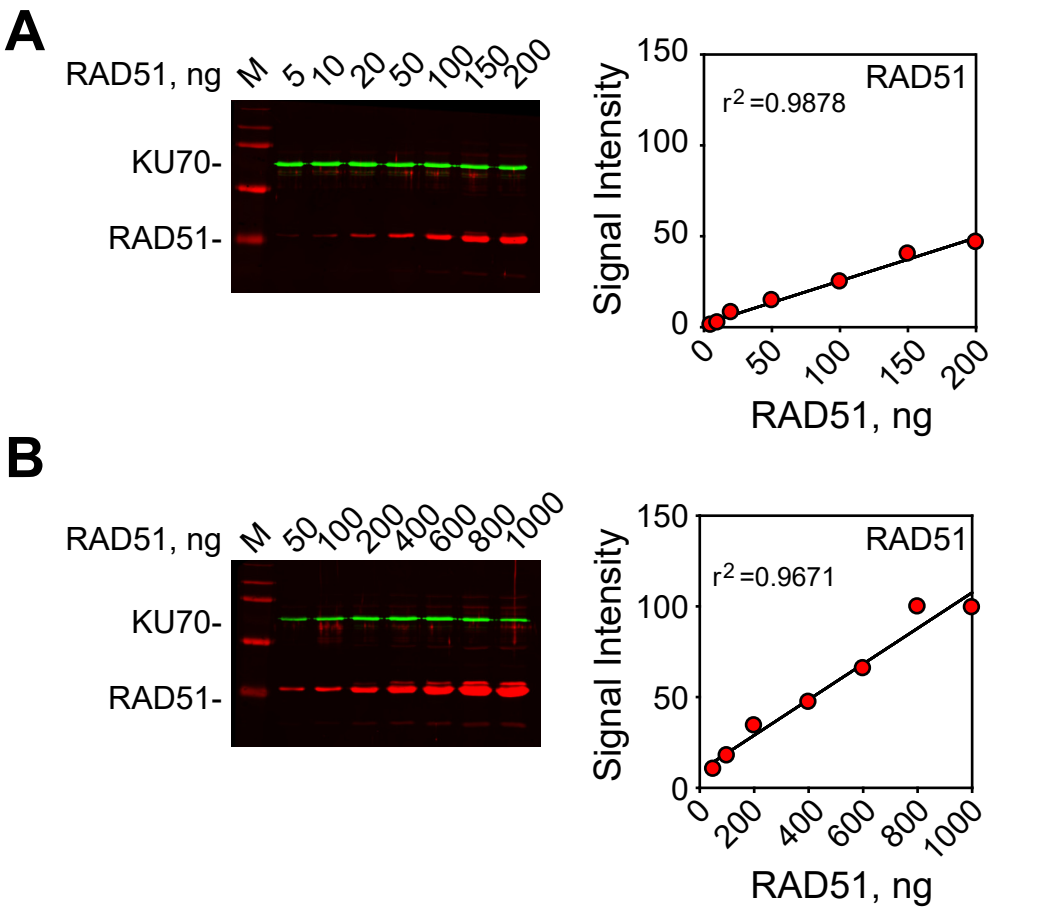


**Figure S5; Mladenov et al.**

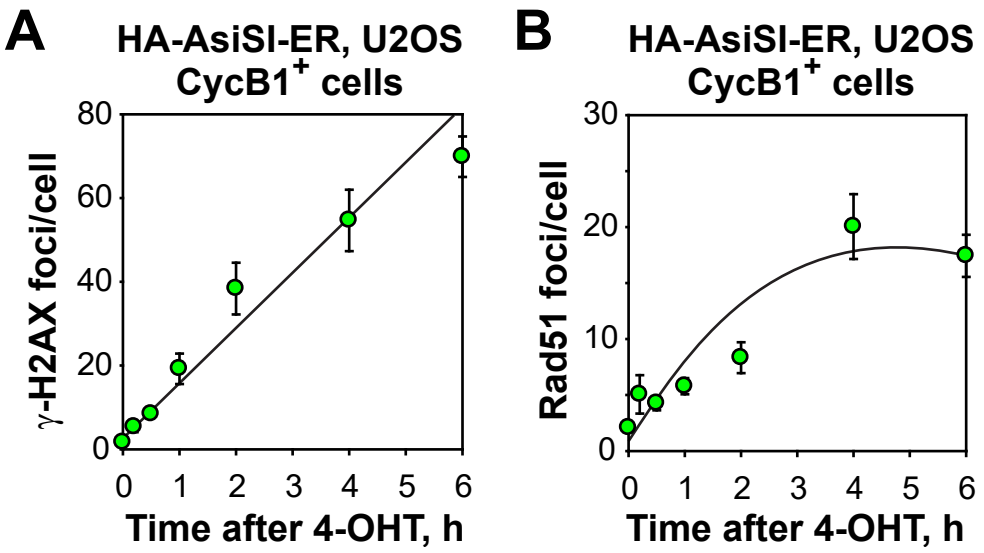


**Figure S6; Mladenov et al.**

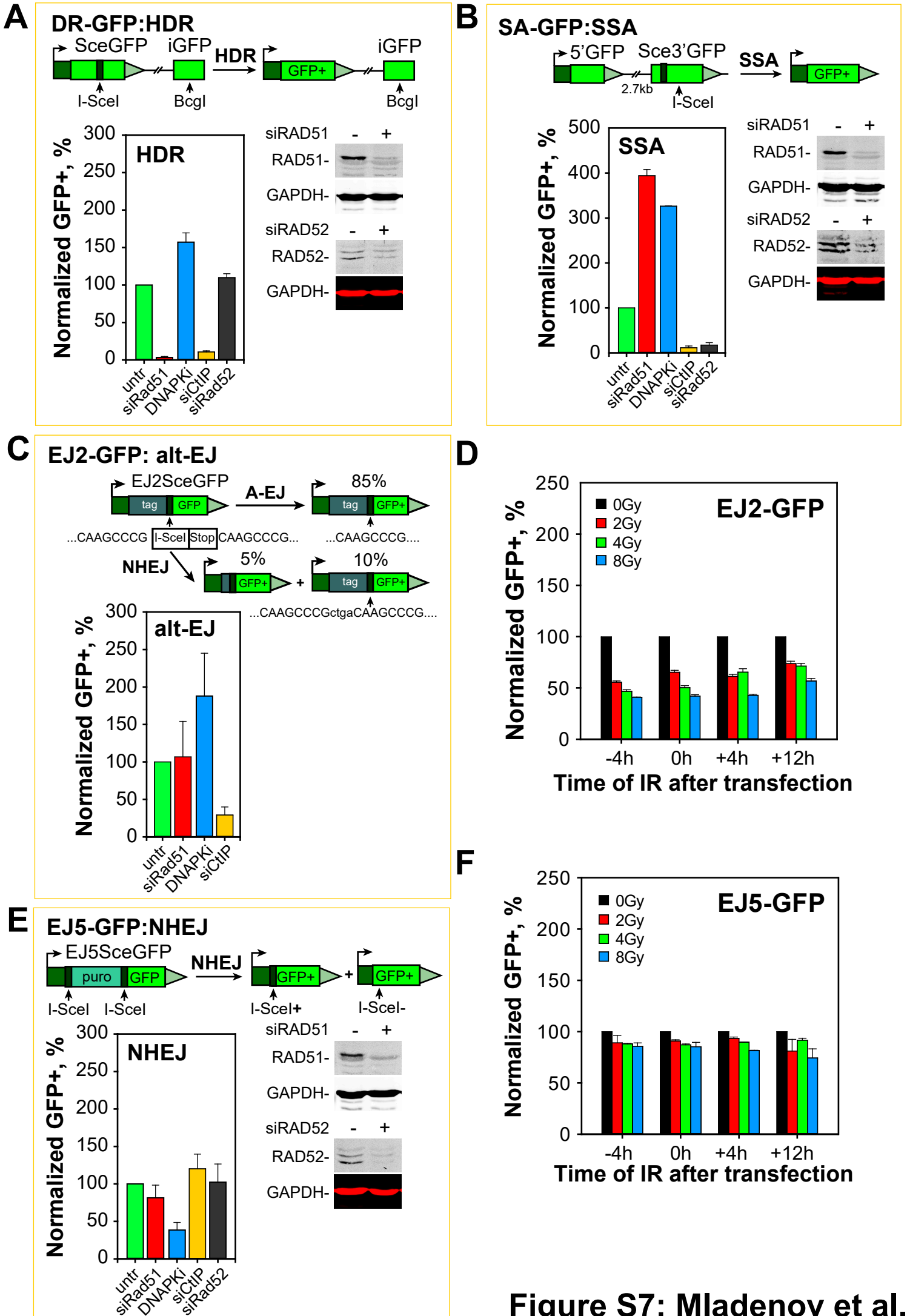


**Figure S7; Mladenov et al.**

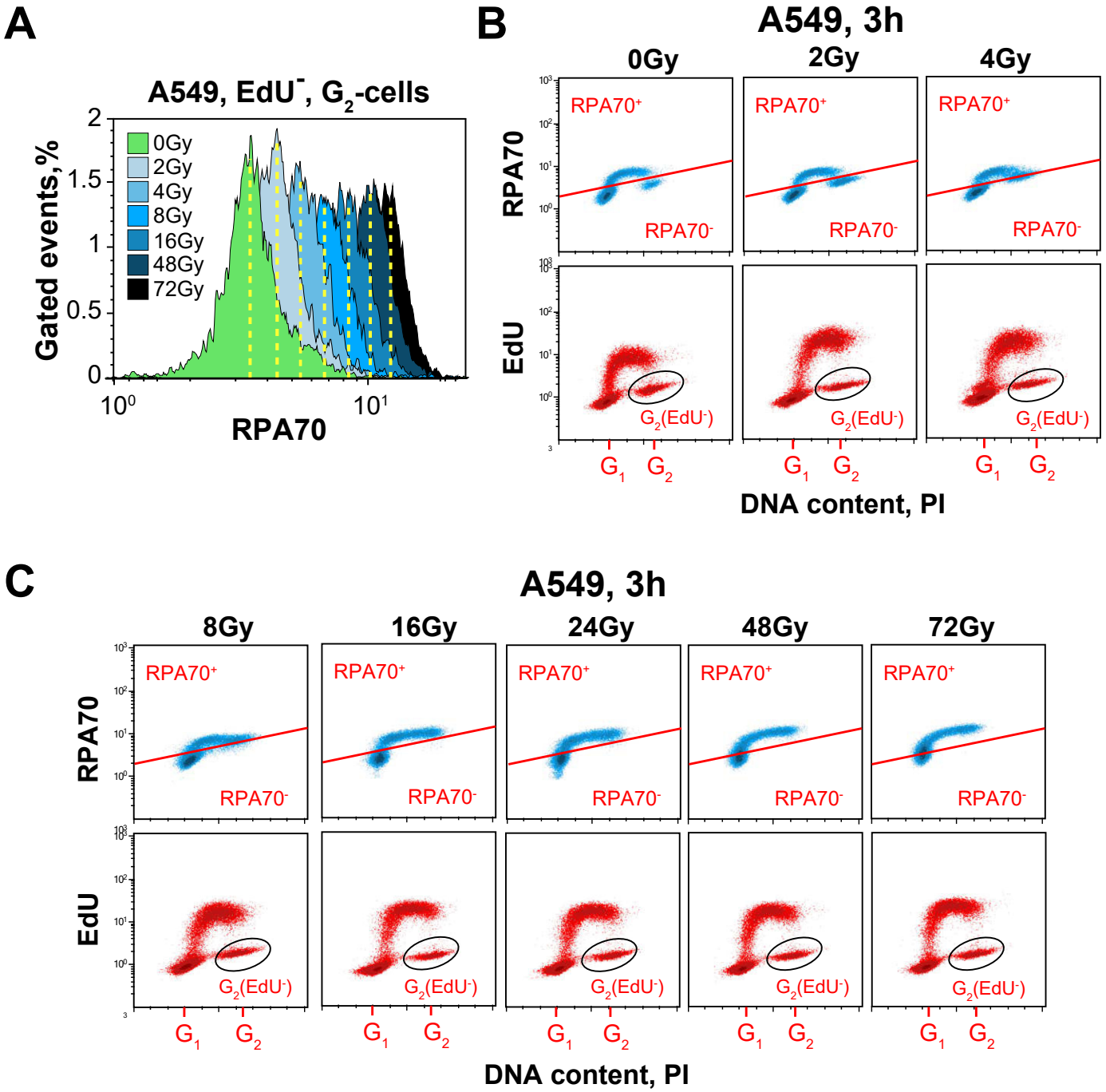


**Figure S8; Mladenov et al.**

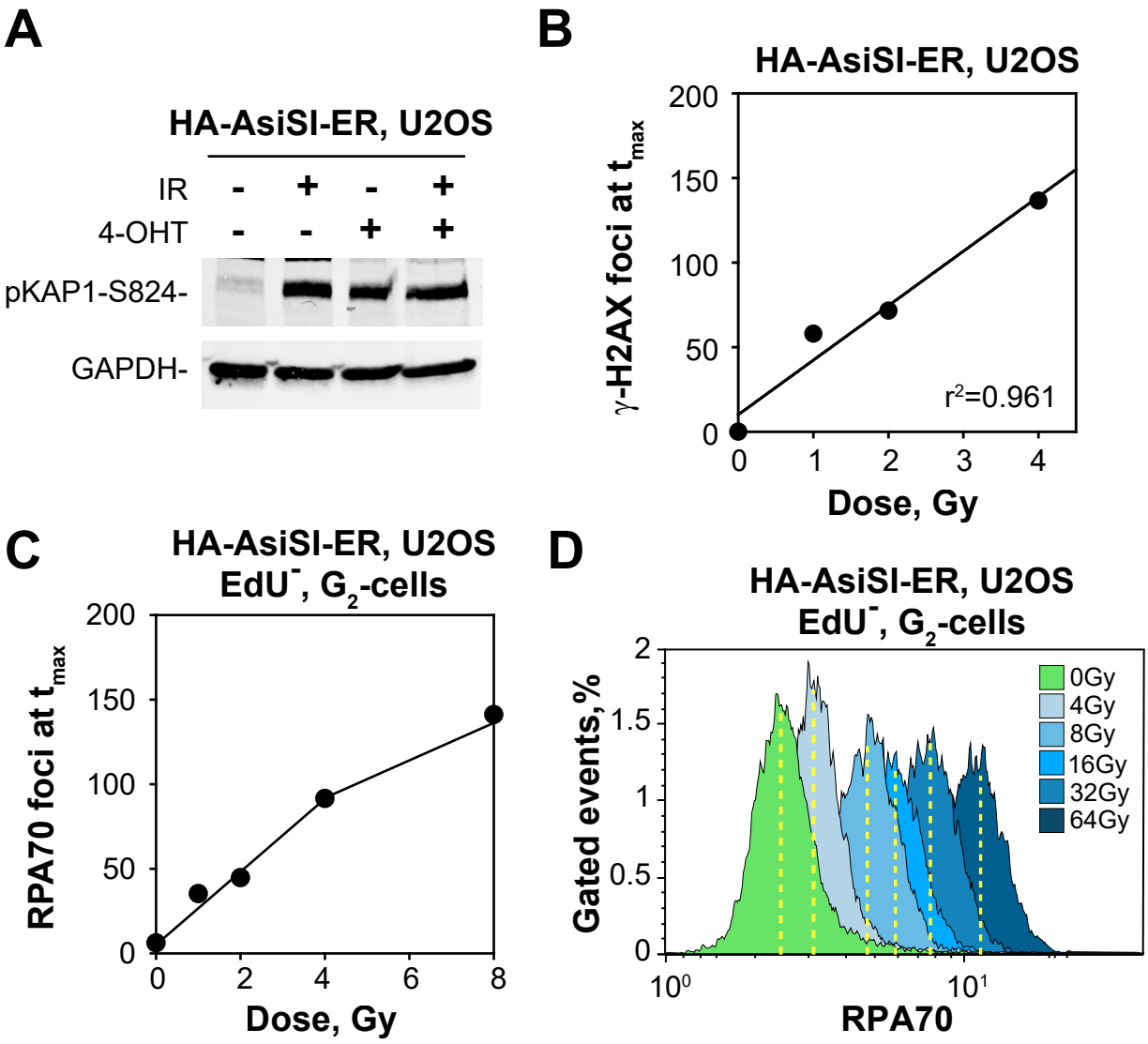


**Figure S9; Mladenov et al.**

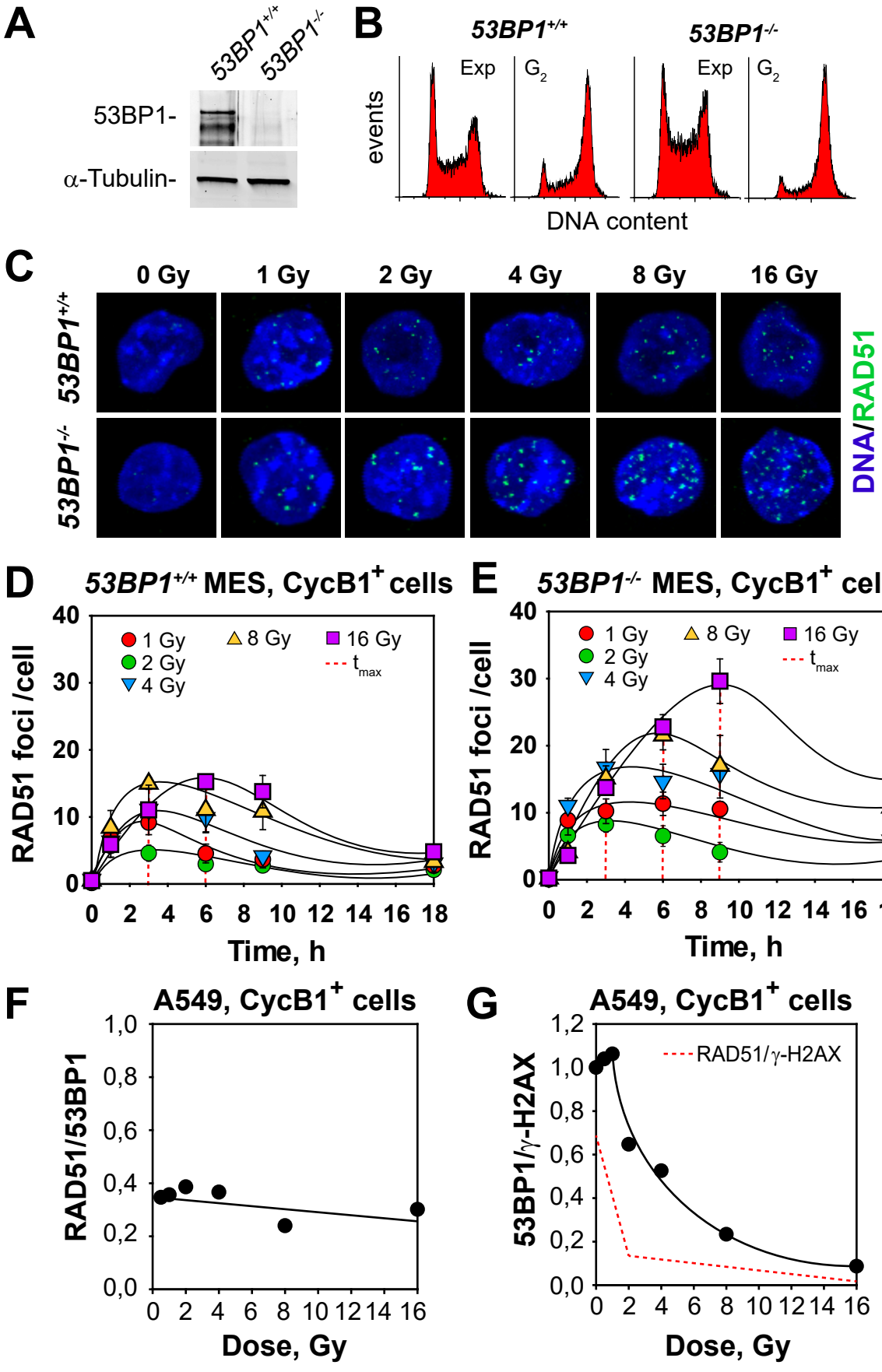


**Figure S10; Mladenov et al.**

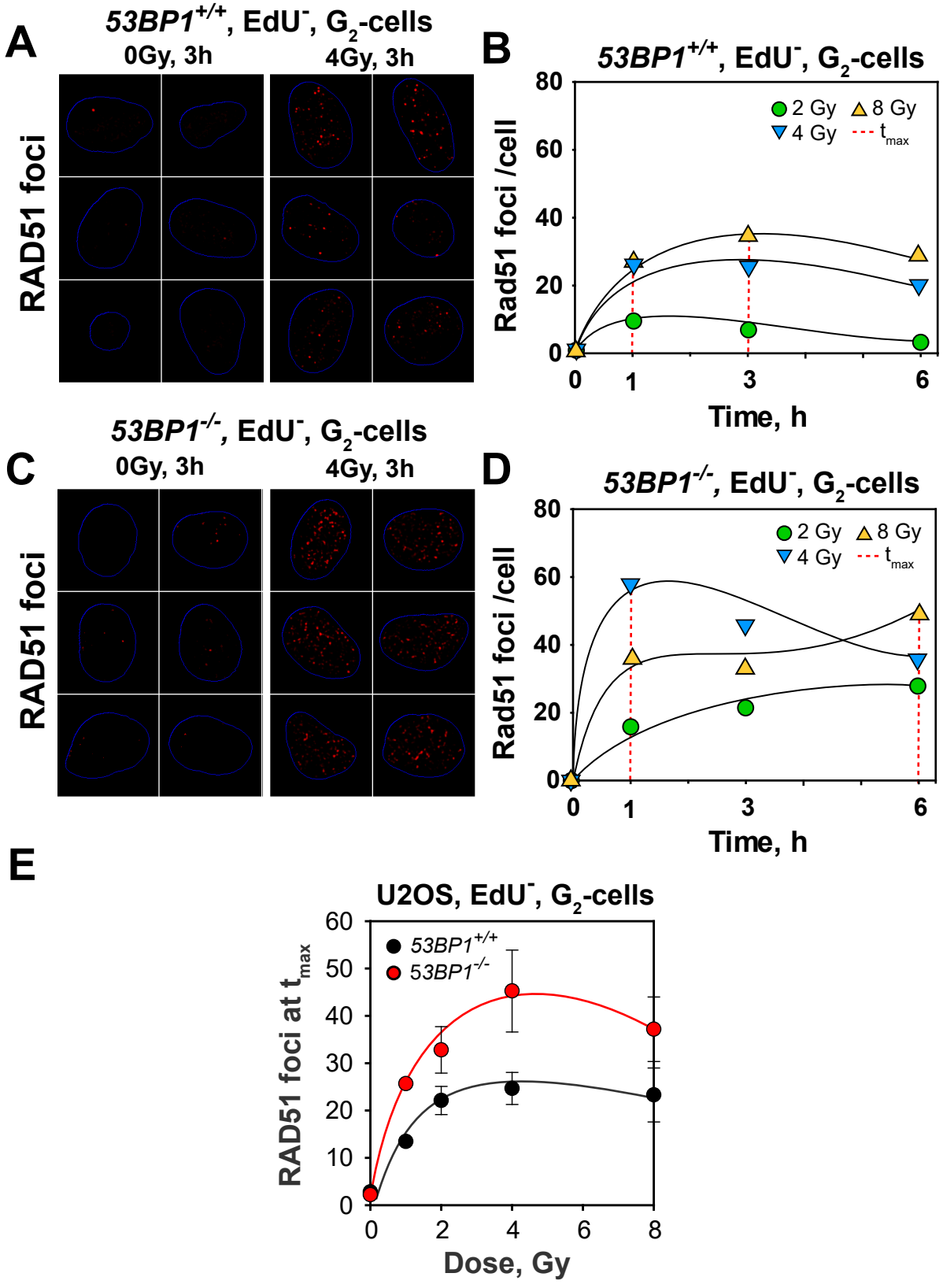


**Figure S11; Mladenov et al.**

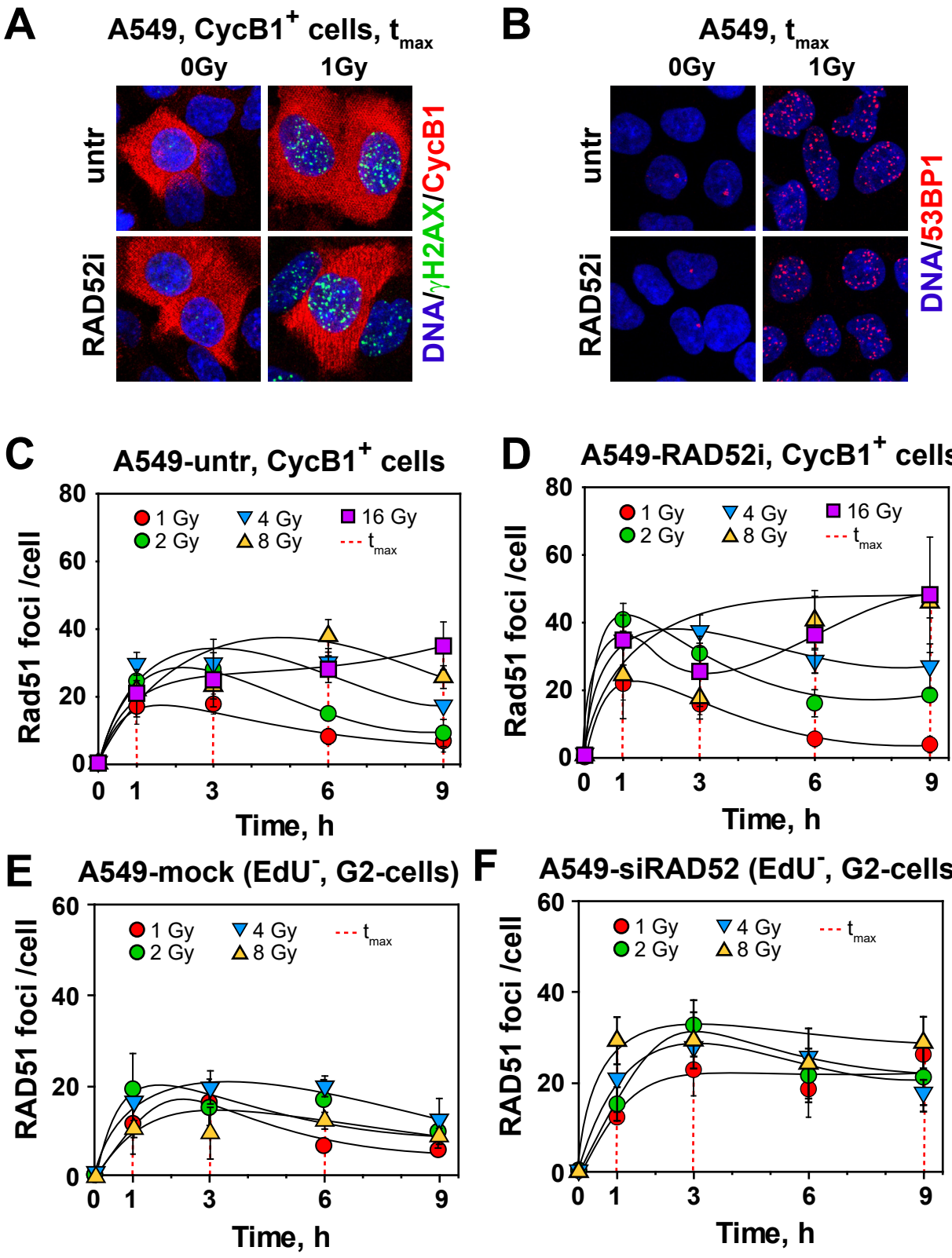


**Figure S12; Mladenov et al.**

**A**

| *pValue, ctrl vs IR* | | | | |
|---|---|---|---|---|
| DR-GFP | -4h | 0h | +4h | +12h |
| | 0Gy | 0Gy | 0Gy | 0Gy |
| 2Gy | 0.1593 | 0.2955 | 0.0337 | 0.0087 |
| 4Gy | 0.03 | 0.0259 | 0.006 | 0.0066 |
| 8Gy | 0.008 | 0.013 | 0.0004 | 0.0011 |
| 16Gy | 0.0045 | 0.0074 | 0.0003 | 0.0003 |
| 32Gy | 0.0021 | 0.0042 | 0.0001 | 0.0001 |

| *pValue, ctrl vs IR* | | | | |
|---|---|---|---|---|
| SA-GFP | -4h | 0h | +4h | +12h |
| | 0Gy | 0Gy | 0Gy | 0Gy |
| 2Gy | 0.5096 | 0.3962 | 0.436 | 0.0197 |
| 4Gy | 0.7373 | 0.6552 | 0.0413 | 0.0456 |
| 8Gy | 0.8288 | 0.0045 | 0.0001 | 0.0009 |
| 16Gy | 0.8032 | 0.0349 | 0.0008 | 0.0012 |
| 32Gy | | | | |

**B**

| *p-Value, mock, ctrl vs IR* | | |
|---|---|---|
| SA-GFP | +4h | +8h |
| | 0Gy | 0Gy |
| 4Gy | 0.2912 | 0.3523 |
| 8Gy | 0.0004 | 0.0014 |
| 16Gy | 0.0001 | 0.0016 |

| *p-Value, siRAD51, ctrl vs IR* | | |
|---|---|---|
| SA-GFP | +4h | +8h |
| | 0Gy | 0Gy |
| 4Gy | 0.7124 | 0.1979 |
| 8Gy | 0.4851 | 0.1979 |
| 16Gy | 0.4461 | 0.176 |

| *p-Value, siRAD52, ctrl vs IR* | | |
|---|---|---|
| SA-GFP | +4h | +8h |
| | 0Gy | 0Gy |
| 4Gy | 0.00273 | 0.6781 |
| 8Gy | 0.2968 | 0.1224 |
| 16Gy | 0.0863 | 0.0675 |

| *p-Value, mock, ctrl vs IR* | | |
|---|---|---|
| DR-GFP | +4h | +8h |
| | 0Gy | 0Gy |
| 4Gy | 0.009 | 0.0162 |
| 8Gy | 0.0051 | 0.0266 |
| 16Gy | 0.0062 | 0.0079 |

| *p-Value, siRAD51, ctrl vs IR* | | |
|---|---|---|
| DR-GFP | +4h | +8h |
| | 0Gy | 0Gy |
| 4Gy | 0.2738 | 0.2138 |
| 8Gy | 0.0556 | 0.0537 |
| 16Gy | 0.03 | 0.044 |

| *p-Value, siRAD52, ctrl vs IR* | | |
|---|---|---|
| DR-GFP | +4h | +8h |
| | 0Gy | 0Gy |
| 4Gy | 0.8449 | 0.0631 |
| 8Gy | 0.0141 | 0.0577 |
| 16Gy | 0.0476 | 0.0318 |

**C**

| p-Value, *mock vs siRAD51* | | | | |
|---|---|---|---|---|
| SA-GFP, +4h | | | | |
| | 0Gy | 4Gy | 8Gy | 16Gy |
| 0Gy | 0.0448 | | | |
| 4Gy | | 0.0125 | | |
| 8Gy | | | 0.0103 | |
| 16Gy | | | | 0.9604 |

| SA-GFP, +8h | | | | |
|---|---|---|---|---|
| | 0Gy | 4Gy | 8Gy | 16Gy |
| 0Gy | 0.0527 | | | |
| 4Gy | | 0.035 | | |
| 8Gy | | | 0.0388 | |
| 16Gy | | | | 0.608 |

| p-Value, *mock vs siRAD52* | | | | |
|---|---|---|---|---|
| SA-GFP, +4h | | | | |
| | 0Gy | 4Gy | 8Gy | 16Gy |
| 0Gy | 0.008 | | | |
| 4Gy | | 0.0001 | | |
| 8Gy | | | 0.0003 | |
| 16Gy | | | | 0.0003 |

| SA-GFP, +8h | | | | |
|---|---|---|---|---|
| | 0Gy | 4Gy | 8Gy | 16Gy |
| 0Gy | 0.0048 | | | |
| 4Gy | | 0.0045 | | |
| 8Gy | | | 0.0009 | |
| 16Gy | | | | 0.0061 |

**D**

| p-Value, *mock vs siRAD51* | | | | |
|---|---|---|---|---|
| DR-GFP, +4h | | | | |
| | 0Gy | 4Gy | 8Gy | 16Gy |
| 0Gy | 0.0055 | | | |
| 4Gy | | 0.0003 | | |
| 8Gy | | | 0.0022 | |
| 16Gy | | | | 0.0349 |

| DR-GFP, +8h | | | | |
|---|---|---|---|---|
| | 0Gy | 4Gy | 8Gy | 16Gy |
| 0Gy | 0.0059 | | | |
| 4Gy | | 0.0232 | | |
| 8Gy | | | 0.0228 | |
| 16Gy | | | | 0.0318 |

| p-Value, *mock vs siRAD52* | | | | |
|---|---|---|---|---|
| DR-GFP, +4h | | | | |
| | 0Gy | 4Gy | 8Gy | 16Gy |
| 0Gy | 0.0283 | | | |
| 4Gy | | 0.0155 | | |
| 8Gy | | | 0.0124 | |
| 16Gy | | | | 0.0331 |

| DR-GFP, +8h | | | | |
|---|---|---|---|---|
| | 0Gy | 4Gy | 8Gy | 16Gy |
| 0Gy | 0.0125 | | | |
| 4Gy | | 0.0082 | | |
| 8Gy | | | 0.6356 | |
| 16Gy | | | | 0.0241 |

**Table S1; Mladenov et al.**